applied optics

Three-dimensional ray tracing in spherical and elliptical generalized Luneburg lenses for application in the human eye lens

J. E. Gómez-Correa,[1,3,*] V. Coello,[1] A. Garza-Rivera,[2] N. P. Puente,[3] and S. Chávez-Cerda[2,4]

[1]Centro de Investigación Científica y de Educación Superior de Ensenada, Unidad Monterrey, Alianza Centro 504, PIIT Apodaca, Nuevo León 66629, Mexico
[2]Instituto Nacional de Astrofísica, Óptica y Electrónica, Luis Enrique Erro No.1, Tonantzintla, Puebla 72840, Mexico
[3]Universidad Autónoma de Nuevo León, Facultad de Ingeniería Mecánica y Eléctrica, Avenida Universidad s/n. Ciudad Universitaria San Nicolás de los Garza, Nuevo León C.P. 66451, Mexico
[4]Centro de Investigaciones en Optica, Loma del Bosque 115, León, Gto. 37150, Mexico
*Corresponding author: jesusg@cicese.mx

Received 24 November 2015; revised 25 January 2016; accepted 9 February 2016; posted 10 February 2016 (Doc. ID 254514); published 10 March 2016

Ray tracing in spherical Luneburg lenses has always been represented in 2D. All propagation planes in a 3D spherical Luneburg lens generate the same ray tracing, due to its radial symmetry. A geometry without radial symmetry generates a different ray tracing. For this reason, a new ray tracing method in 3D through spherical and elliptical Luneburg lenses using 2D methods is proposed. The physics of the propagation is shown here, which allows us to make a ray tracing associated with a vortex beam. A 3D ray tracing in a composite modified Luneburg lens that represents the human eye lens is also presented.

OCIS codes: (330.0330) Vision, color, and visual optics; (080.2710) Inhomogeneous optical media; (080.5692) Ray trajectories in inhomogeneous media; (110.2760) Gradient-index lenses; (330.7326) Visual optics, modeling; (080.1753) Computation methods.

http://dx.doi.org/10.1364/AO.55.002002

1. INTRODUCTION

The most famous lens with a gradient refractive index (GRIN) is the spherical Luneburg lens. This lens was introduced in 1944 by Rudolf K. Luneburg in the book *Mathematical Theory of Optics* [1]. A Luneburg lens is a GRIN lens with spherical geometry with a normalized unitary radius and stigmatic properties, which focus a sphere into a sphere [2]. As a particular example, Luneburg solved the problem for incident rays, at the anterior surface, coming from infinity (infinite sphere), thus focusing at the opposite side surface of the spherical lens (sphere with radius $r = 1$). The Luneburg lens is a remarkable optical lens because it is an aberration-free lens.

In telecommunications, it is difficult to apply the spherical Luneburg lens in any practical antenna system due to its large spherical shape. For this reason, a transformation that reduces the profile of the original Luneburg lens without affecting its unique properties [3,4] has been recently proposed. The new transformed slim lens is then discretized and simplified for practical antenna applications [3].

The spherical Luneburg lens and the ellipsoidal Luneburg lens have been designed experimentally using Polymeric nanolayered materials. The first lens is presented as a developing application of the nanolayered polymer technology [5], and the second lens is used to model a human eye lens using the anterior and posterior shapes [6] because this lens is considered an asymmetric GRIN lens.

Many generic expressions for the refractive index based on biometric data of animal and human lenses have been proposed over the years, which provide a good estimation of the actual GRIN distribution [7–9]. In some models, the anterior and posterior faces are considered to be symmetric [7], while, in more recent models, a realistic asymmetry of the faces is taken into account [8,9]. In the latter, the GRIN is described by two different equations with respect to a plane or a curved surface that intersects the human lens at its equator [8–10]. A drawback is that a ray (or its derivative) traveling in the proposed GRIN distribution may undergo a discontinuity at any of such surfaces.

It has been demonstrated that the human eye lens could be represented as a lens based on the gradient-index Luneburg lens and composed of two oblate half-spheroids of different curvatures that have continuous isoindicial contours and that incorporate curvatures and which are similar to those found in a human lens. This lens was called a composite modified Luneburg (CML) lens [11].

The human eye lens and the Luneburg lenses can be studied using geometrical optics, but, to the best of our knowledge, ray

tracing methods have only been performed in 2D, and the ray tracing is along the sagittal plane of these lenses [4,8,11–15].

It is possible to perform ray tracing in 3D in Luneburg lenses or in GRIN lenses using commercial optical design software. Unfortunately, for some users, they are like a black box. It is common to think that, by using entry parameters, a correct simulation could be performed, but the physics inside the lenses that generate the ray tracing is not clear. In more complicated cases, it is necessary to know the physics of the problem to obtain a better explanation of the solution.

An example of a complex problem is the human eye lens. This lens has been studied in 2D using commercial software [8,12]. However, for 3D ray tracing, it is necessary to know the physics of the ray path because the human eye lens is not symmetrical, and a better analysis could be made.

In this paper, ray tracing and its physical explanation in 3D of the spherical and elliptical Luneburg lenses based on the well-known methods in 2D are presented. Thus, using the proposed method, 3D ray tracing in a CML lens that represents the human eye lens is also presented.

2. SPHERICAL LUNEBURG LENS: 3D GEOMETRY OF THE GRIN DISTRIBUTION AND 3D RAY TRACING

The index in the spherical Luneburg lens is described as a function of $n(r)$ where $r = \sqrt{x^2 + y^2 + z^2}$ and x, y, and z are Cartesian coordinates. This function represents a refractive index that is constant in concentric spherical shells, i.e., each shell has a thickness of dr ($dr \to 0$), and, in this thickness, the refractive index is constant. The smallest sphere has the highest refractive index, and this value decreases from the inner shell to a shell of radius a (this last shell is the surface of the lens) (see Fig. 1).

If we assume that the GRIN distribution in the spherical Luneburg lens has rotational symmetry around of the z axis, we can define $\rho = \sqrt{y^2 + z^2}$ where ρ is the projection of r in the y–z plane. This plane is defined as the sagittal plane of the spherical Luneburg lens, and its GRIN distribution is given by $n(\rho)$. The function $n(\rho)$ implies that the GRIN distribution is not spherical where the refractive index is constant, which means that the GRIN distribution is composed of circles with a constant refractive index.

The sagittal plane is represented by the red circle in Fig. 2. From this plane, it is possible to generate the GRIN distribution $n(r)$, if we make a rotation of $\phi_r = 2\pi$ radians of the sagittal semiplane given by $y > 0$ with respect to the z axis or if we make a rotation of $\beta_r = 2\pi$ radians of the sagittal semiplane given by $z > 0$ with respect to the y axis, where ϕ_r and β_r are representing the rotation angles with respect to the z and y axis, respectively, as shown in Fig. 2. The GRIN distribution of the sagittal semiplane acts as a solid of revolution; the semicircles rotation generates a spherical GRIN distribution.

Without losing generality, both $n(r)$ and r could be normalized with respect to the maximum value of $n(r)$, and r, i.e., with respect to $n(a)$ and a, respectively. The values of the GRIN distribution and the radius on the surface of the sphere are the unit [14].

The ray paths along a GRIN distribution of spherical symmetry could be described by means of the Eikonal equation, which is given in terms of the polar and radial coordinates as

$$\left(\frac{\partial \psi}{\partial r}\right)^2 + \frac{1}{r^2}\left(\frac{\partial \psi}{\partial \theta}\right)^2 = n^2(r), \tag{1}$$

where the surfaces $\psi =$ constant are associated with the optical wavefronts. This Eikonal equation could be solved using separation of variables, and, to obtain an equation describing any ray, it is necessary to apply the Jacobi theorem to the solution because the solution of Eq. (1) describes the optical wavefronts, and the polar equation of any ray could be written in terms of a single equation given by

$$\theta_s - \theta_i = \pm K \int_{r_0}^{r} \frac{\mathrm{d}r}{r\sqrt{n^2(r)r^2 - K^2}}, \tag{2}$$

where (r_0, θ_i) are the coordinates of the point of a ray entry into the lens, as shown in Fig. 3, and K is the separation constant. The expression for K could be found by calculating the derivative of Eq. (2) with respect to the radial coordinate, i.e.,

$$K = n(r) r \sin \varphi. \tag{3}$$

In this expression, the angle φ is formed between the radial vector and the tangent to the ray path [1] (see Fig. 3). The

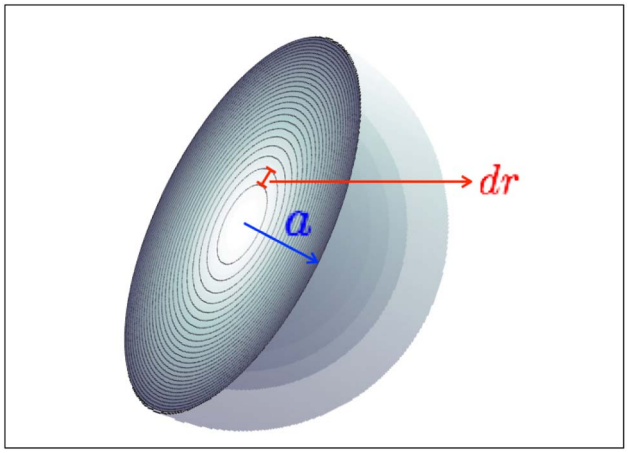

Fig. 1. GRIN distribution in the spherical Luneburg lens.

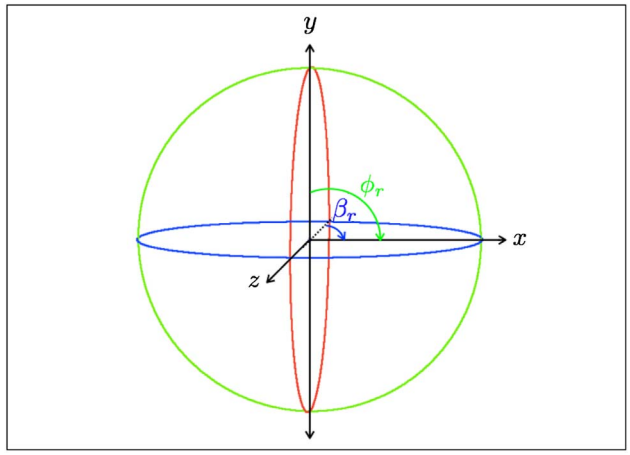

Fig. 2. Spherical Luneburg lens geometry.

value of K could be obtained straightforwardly at the surface of the lens:

$$K = n_0 r_0 \sin \alpha_0, \tag{4}$$

where n_0 is the refractive index value on the surface of the lens, and α_0 is the angle formed by the ray with the optical axis (see Fig. 3). Due to a normalization, this value has a variation from 0 to 1, i.e., $0 \le K \le 1$.

From Eq. (4), it is possible to observe that, for each ray, exists a unique value of K. This value remains constant along the ray path [16–18].

The expression given by Eq. (3) is known as the generalized Snell law for inhomogeneous media, and its values determine the optical path of each ray. This demonstrates that the paths of rays in a medium with gradient index $n = n(r)$ are planar curves, situated in a plane through the origin because K is always a constant with a positive or negative sign, and there is no sign change along the ray [19]. This plane is defined as the ray propagation plane.

The last paragraph is important because it gives us the idea of how to make a 3D ray tracing inside a lens with a GRIN distribution given by $n = n(r)$. It also gives us the idea of the technical difficulties that are present in 2D and 3D ray tracing. In 2D ray tracing in Luneburg lenses, the technical difficulties are reduced to knowing the value of the constant K for each incident ray, which depends on the entry point in a single plane; in this case, it is in the propagation plane. However, in 3D ray tracing, the technical difficulties are tripled compared with 2D ray tracing. It is necessary to know which is the propagation plane for an incident ray; thus, it is crucial to find the value of the constant K in each propagation plane for any incident ray. These parameters depend on the incident ray direction. It is necessary to know if it is a meridional ray or if it is not a meridional ray (skew ray). For this reason, it is necessary to know the propagation plane; therefore, we will have to characterize it in the following paragraphs.

Ultimately, 3D ray tracing is necessary to define an entry point of a ray into the lens in 3D. This point is given by $P_{iL} = (r_{iL}, \theta_{iL}, \phi_{iL})$, where ($r$, θ, and ϕ) are spherical coordinates in the x–y–z reference frame. From Fig. 4, it could be observed that the entry ray is on the surface of the sphere. This implies that $r_{iL} = 1$, so the entry point is reduced to $P_{iL} = (1, \theta_{iL}, \phi_{iL})$.

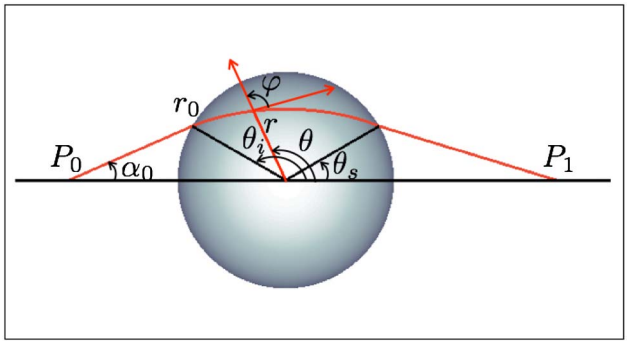

Fig. 3. Luneburg lens showing the geometric parameters of the ray path.

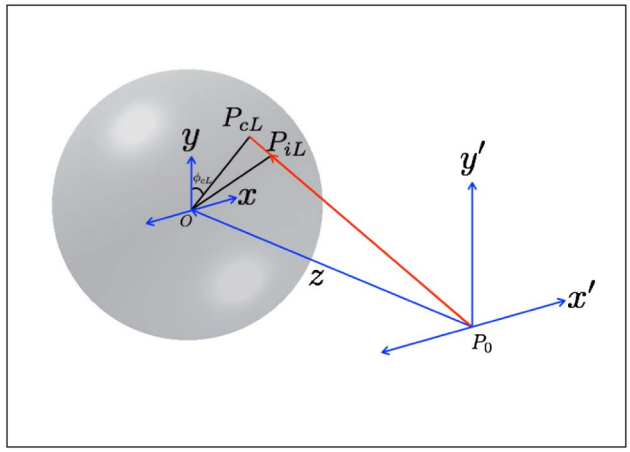

Fig. 4. Luneburg lens showing the geometric parameters of the 3D ray path.

At this point, the entry point of the ray in the sphere has been defined, but the ray propagation plane has not yet been specified. This plane is easier to find, if a new point inside of the sphere is located. Three points on the ray propagation plane will be given, and, with these three points, a normal vector to the plane that fully defines the ray propagation plane could be found. This point is defined in the xy plane when the incident ray is extended to this plane. The point is represented as P_{cL} in Fig. 4, and its coordinates are given by $P_{cL} = (r_{cL}, \pi/2, \phi_{cL})$. It is important to say that the extension of the ray's extension inside the lens is not the ray propagation in a medium with gradient index $n = n(r)$, the extension is only to define the ray propagation plane.

With the points O, P_{cL}, and P_{iL}, a normal vector to the ray propagation plane in spherical coordinates could be found. This is shown by

$$\vec{n} = \left(\frac{\pi}{2}\phi_{iL} - \phi_{cL}\theta_{iL}\right)\hat{r} + (\phi_{cL} - r_{cL}\phi_{iL})\hat{\theta} + \left(r_{cL}\theta_{iL} - \frac{\pi}{2}\right)\hat{\phi}, \tag{5}$$

where $\hat{r}$, $\hat{\theta}$, and $\hat{\phi}$ are the unit vectors in spherical coordinates. Using this normal vector, this plane could be represented as

$$\left(\frac{\pi}{2}\phi_{iL} - \phi_{cL}\theta_{iL}\right)r + (\phi_{cL} - r_{cL}\phi_{iL})\theta + \left(r_{cL}\theta_{iL} - \frac{\pi}{2}\right)\phi = d, \tag{6}$$

where $d = (\frac{\pi}{2}\phi_{iL} - \phi_{cL}\theta_{iL})r_{cL} + (\phi_{cL} - r_{cL}\phi_{iL})\theta_{cL} + (r_{cL}\theta_{iL} - \frac{\pi}{2})\phi_{cL}$, and it is a constant.

The ray propagation plane for any ray is expressed by Eq. (6), and the gradient index is given by $n(r)$. This is enabled by the spherical geometry of the Luneburg lens because any plane passing through the origin will have this gradient index.

In Fig. 3, the point P_0 represents the coordinates where the source point (object point) is placed. This point is placed at the optical axis of the lens. It is important to say that Eq. (6) allows us to find any propagation plane for any incoming ray from a source point placed at any point of the 3D space. If the point is placed at the optical axis, the propagation plane is easily found for each ray because the propagation planes are defined by the two parameters given in Fig. 2, and its values are

$$\phi_r = \phi_{cL}$$
$$\beta_r = 0. \quad (7)$$

As the propagation plane is known, it is possible to make the 3D ray tracing with a 2D method because the 3D problem is transformed into a 2D problem using the idea that the rays in a medium with gradient index $n = n(r)$ are planar curves situated in a plane through the origin [19]. It could be observed that the points O, P_{cL}, and P_{iL} were only used for the calculation of the propagation plane. And, with this analysis of the propagation plane, one technical difficulty was solved. The problem of knowing which is the value of the constant K was solved using Eq. (4). Thus, the difficulty of the direction of the rays in this section is not necessary to solve because the classical Luneburg lens has a spherical symmetry. But, in the next section, an analysis of the ray direction is made, due to elliptical symmetry of the Luneburg lens.

Let us create examples using this theory; thus, it will be considered that the point P_0 is placed at the optical axis because it is one of the principles of the Luneburg lens. The first example is the classical spherical Luneburg lens. If the rays are propagating in a GRIN distribution of $n(r) = \sqrt{2 - (\frac{r}{a})^2}$ and the entry parameters shown in Fig. 3 are given by $\alpha_0 = 0$ and $r_0 = 1$, the parameter $\alpha_0 = 0$ thus implies that the point P_0 is placed at infinity. The parameter θ_i has the same value for each ray on its propagation plane.

Three-dimensional ray tracing in the classical spherical Luneburg lens is shown in Fig. 5(a). The rays outside the lens are represented in red, and the rays inside the lens are represented in blue. Figure 5(b) represents the 3D ray tracing projection in the sagittal plane, and Fig. 5(c) represents 2D ray tracing in the same plane.

In Fig. 5(b), it could be expected to see that all the rays coming from infinity are entering the lens along the anterior section of a circle, as is shown in Fig. 5(c) (red circle), but this is not possible because, in Fig. 5(b), the rays are entering in different planes, and only the rays represented with dashed lines are entering in the sagittal plane. In Fig. 5(c), all rays are entering in the sagittal plane along the anterior section of the red circle.

The second and last example in this section is when the ray tracing for a generalized spherical Luneburg lens is performed. In this example, point P_0 is placed at a different distance from infinity and point P_1 is different to 1. In this case, it is necessary to modify the gradient refractive index because the geometry of the lens is the same as that in the first example [4,11].

In this example, the entry parameters are given by $P_0 = 5$ and $r_0 = 1$. If all rays should be focused at the point $P_1 = 1.37$, the refractive index must be

$$n(r) = \sqrt{1.8 - \left(\frac{r}{a}\right)^2}, \quad (8)$$

which ranges from 1.3416 in the center to 1 in the surface of the sphere. The 3D ray tracing of the generalized spherical Luneburg lens is shown in Fig. 6; thus, it could be observed that all rays are practically focused on the image plane at a distance of 1.37 units from the center of the sphere.

3. ELLIPTICAL LUNEBURG LENS: 3D GEOMETRY OF THE GRIN DISTRIBUTION AND 3D RAY TRACING

From the spherical Luneburg lens, it is possible to make a linear transformation and to obtain the elliptical Luneburg lens without affecting its unique properties [3,4,11].

The index in the spherical Luneburg lens is described by Eq. $n(r)$, but if symmetry around the y axis is assumed, then the desired elliptical shape could be obtained when the radius is defined as

$$r = \sqrt{\left(\frac{1}{s}x\right)^2 + y^2 + \left(\frac{1}{s}z\right)^2}, \quad (9)$$

where s is a constant and the 3D GRIN distribution in the elliptical Luneburg lens is given by

$$n(r) = \sqrt{2 - \left[\left(\frac{1}{s}x\right)^2 + y^2 + \left(\frac{1}{s}z\right)^2\right]}, \quad (10)$$

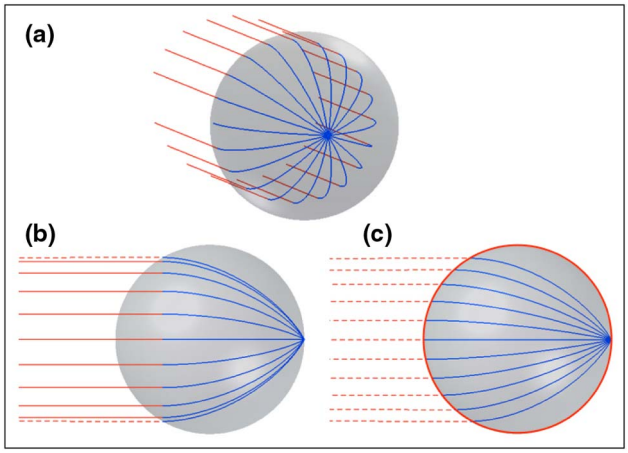

Fig. 5. 3D ray tracing in the classical spherical Luneburg lens. (a) The observation angle allows us to observe the 3D ray tracing. (b) The 3D ray propagating is observed on the sagittal plane. (c) 2D ray tracing in the sagittal plane.

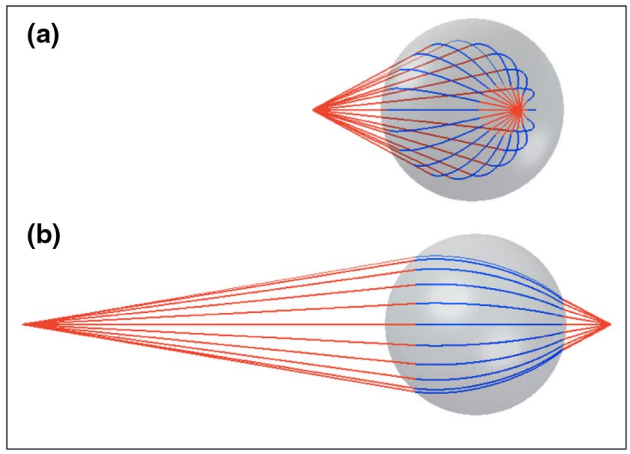

Fig. 6. 3D ray tracing in the generalized spherical Luneburg lens. The 3D ray propagation is observed on (a) an angle that allows us to observe the 3D ray tracing and (b) the sagittal plane (zy plane).

where this function represents a refractive index that is constant on concentric elliptic shells. The GRIN distribution on the sagittal plane (yz plane) is shown in Fig. 7; in this case, $x = 0$ and r is transformed as $\rho = \sqrt{y^2 + (\frac{1}{s}z)^2}$.

The 3D GRIN distribution of the elliptical Luneburg lens could be generated in two ways. The first is when a rotation of $\beta_r = 2\pi$ radians of the sagittal semiplane given by $z > 0$ with respect to the y axis is done, as is shown in Fig. 8. This is possible because, from the beginning symmetry, the y axis was considered. The second is when a rotation of $\phi_r = 2\pi$ radians of the sagittal semiplane given by $y > 0$ with respect to the z axis is made. In the case of the elliptical Luneburg lens, if only this rotation is considered, the 3D GRIN distribution could not be generated because the semimajor axis of the sagittal plane could not be a constant due to the elliptical geometry of this lens.

In order to generate the GRIN distribution from this rotation, it is necessary to define, in polar coordinates, a new function for the semimajor axis of sagittal plane that depends on ϕ_r. The semimajor axis in each plane is represented by

$$\rho_V(\phi_r) = \frac{s'}{\sqrt{s'^2 \cos^2 \phi_r + \sin^2 \phi_r}}, \tag{11}$$

where $s' = 1/s$ and its variation is

$$1 \geq \rho_V \geq s'. \tag{12}$$

It is important to see that, when the sagittal plane is rotated in the direction of the angle ϕ_r, the semiminor axis of this plane (ρ_H) remains constant and its value is $\rho_H = s'$.

Using the values of ρ_H and ρ_V for each ϕ_r, it is possible to know the change in the geometry of the sagittal plane when a rotation with respect to the z axis is made. The variation of ϕ_r given by $0 \leq \phi_r \leq \pi/2$ implies that $\rho_V(0) = 1 \geq \rho_V(\phi_r) \geq \rho_H$, i.e., the sagittal plane is losing its ellipticity when ϕ_r increases until it becomes a circle with a radius equal to s' at $\phi_r = \pi/2$, and the variation of ϕ_r from $\pi/2$ to π implies that ellipticity of the sagittal plane increases until it becomes in the initial sagittal plane ($\phi_r = 0$). Each plane is defined by

$$\rho(\phi_r) = \sqrt{\rho_V^2(\phi_r)y^2 + \rho_H^2 z^2}, \tag{13}$$

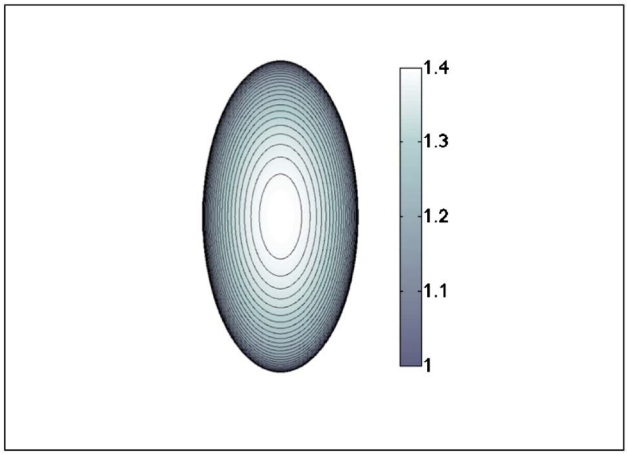

Fig. 7. GRIN distribution in the sagittal plane of the elliptical Luneburg lens.

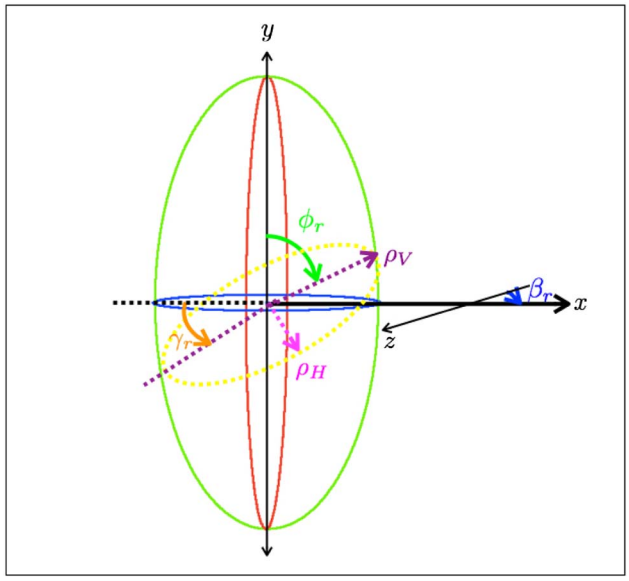

Fig. 8. Elliptical Luneburg lens geometry.

and their GRIN distribution is given by

$$n(\rho(\phi_r)) = \sqrt{2 - [\rho_V^2(\phi_r)y^2 + \rho_H^2 z^2]}, \tag{14}$$

thus, with these two equations, it is possible to generate the 3D GRIN distribution of the elliptical Luneburg lens when a rotation of the sagittal plane with respect to the z axis is done.

Equations (13) and (14) are important for the 3D ray tracing because, if the source point is placed on the optical axis, it could be said that the propagation planes are define by these two equations.

The most general case is when the source point is placed outside of the optical axis; in this case, the propagation planes are described by

$$\rho(\phi_r, \gamma_r) = \sqrt{\rho_V^2(\phi_r)y^2 + \rho_H^2(\gamma_r)z^2}, \tag{15}$$

where γ_r is the angle formed by the propagation plane and the zx plane (see Fig. 8), and

$$\rho_H(\gamma_r) = \frac{s'}{\sqrt{s'^2 \cos^2 \gamma_r + \sin^2 \gamma_r}}, \tag{16}$$

and their GRIN distribution is given by

$$n(\rho(\phi_r, \gamma_r)) = \sqrt{2 - [\rho_V^2(\phi_r)y^2 + \rho_H^2(\gamma_r)z^2]}. \tag{17}$$

Note that point P_0 is placed at the optical axis in the same way as in the spherical Luneburg lens (see Section 2). In the last example of this section, a more general analysis will be made using Eqs. (15) and (17), which represent the geometry and the GRIN of each propagation plane, respectively, when the P_0 point is placed outside the optical axis.

An excellent description of 2D ray tracing in elliptical Luneburg lenses is given in [4]. In this paper, a similar procedure is described, but it is modified accordingly to the propagation in 3D and the desired geometry.

It is considered, in the first two examples of the 3D ray tracing in this section, that the source point is placed on the optical axis. The first example is when the parameters are given by $\alpha_0 = 0$ and $s' = 0.52$. The parameters θ_i and r_0 have different values for each ray on different propagating planes, and its relationship with the ray in the sagittal plane is given by $\theta_i(\phi_r) = \rho_V \theta_i(0)$ and $r_0(\phi_r) = \rho_V r_0(0)$.

Three-dimensional ray tracing in the elliptical Luneburg lens is shown in Fig. 9(a). The chosen geometrical parameter (s') and refractive index $n(r)$ produce practically a perfect focus at the image plane placed at a distance of 1.6 units from the posterior surface of the lens. This image plane could be placed at any point of the optical axis, if we choose the parameters α_0, s' and $n(r)$ in an appropriate manner, i.e., the image plane will depend on these parameters. This propagation could be considered a propagation in a generalized elliptical Luneburg lens because the image plane is outside the lens.

In Figs. 9(b)–9(d), the frontal, sagittal, and tangential propagation planes of the elliptical Luneburg lens could be observed, respectively. The principal difference between the sagittal plane and tangential plane is the geometry of the propagation planes. The first plane has an elliptical geometry, and the second has a circular geometry [see Figs. 9(c) and 9(d), respectively]. In Fig. 9(a), it seems that Snell's law is not fulfilled in most exterior rays, but, in all rays, this law is satisfied, as can be observed in Fig. 9(b). This problem is due to the observation angle in the sagittal plane. In the tangential plane, it could be thought that all the rays should be focused on the surface of the lens because it has a circular geometry and has the same gradient refractive index as that of the spherical Luneburg lens; however, it must be remembered that the spherical Luneburg lens in each plane has a radius that is equal to 1, and, in the tangential plane, the radius is equal to s'; for this reason, the rays could not focus on the surface.

The second example is when point P_0 is placed at $P_0 = 5$; thus, $P_1 = 1.64$ and $s' = 0.44$ imply that the gradient refractive index in each plane is given by

$$n(\rho(\phi_r)) = \sqrt{2.65 - [\rho_V^2(\phi_r)y^2 + s'^2 z^2]}, \tag{18}$$

where the refractive index is varies from 1.6279 to 1. The 3D ray tracing in this media is shown in Fig. 10; thus, it is possible to observe that this media represents a generalized elliptical Luneburg lens because it keeps the unique properties of the Luneburg lens.

In both examples in this section, the set of incident rays on the lenses come from point P_0. The position of this point is different for each example, but both points are placed on the optical axis. If point P_0 is not placed in the optical axis, the entry rays on the ellipse are skew rays. For this reason, an important example to consider is when point P_0 is placed outside the optical axis.

One of the best examples of skew rays propagation in a GRIN medium is the ray propagation inside a cylindrical waveguide with a parabolic refractive index, where the solution is an extreme form of a skew ray, which is known as a helical ray [18]. It is possible to think that the skew rays in an elliptical Luneburg lens are propagated in the same way as the rays inside a cylindrical waveguide with a parabolic refractive index. For the analysis presented in this paper, the propagating rays inside the lens are not skew rays because this lens is immersed in a refractive index n_s, where its value is equal to the value of the refractive index on the surface of the lens. This refractive index allows or does not allow the generation of the skew rays inside of the elliptical Luneburg lens. For example, if the value of the refractive index where the lens is immersed is different from the value of the refractive index on the lens surface, an incident skew ray on the lens generated a propagating skew ray inside this lens due to an immediate refraction in the point where the ray is incident on the lens. However, for the elliptical Luneburg lens proposed in this paper, this refraction does not occur because there is not a difference in the refractive index; this allows the incident skew rays to choose only one propagation plane.

To the set of incident rays on the lenses shown in the two examples of this section, it is possible to associate a plane

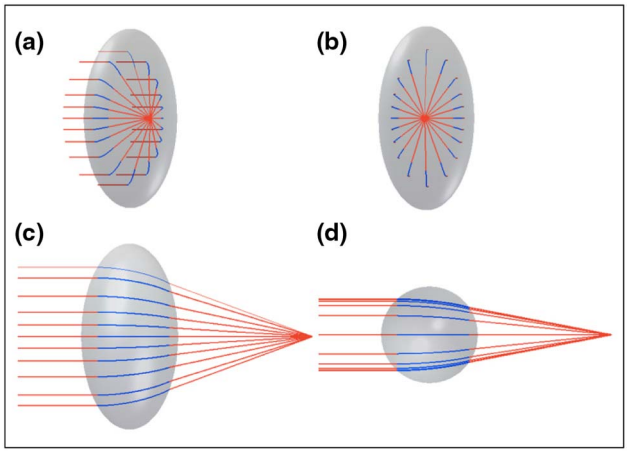

Fig. 9. 3D ray tracing in the generalized elliptical Luneburg lens. The propagating ray is observed in (a) an angle that allows the observation of the 3D ray tracing, (b) the Frontal plane (xy plane), (c) the sagittal plane (zy plane), and (d) the tangential plane (zx plane).

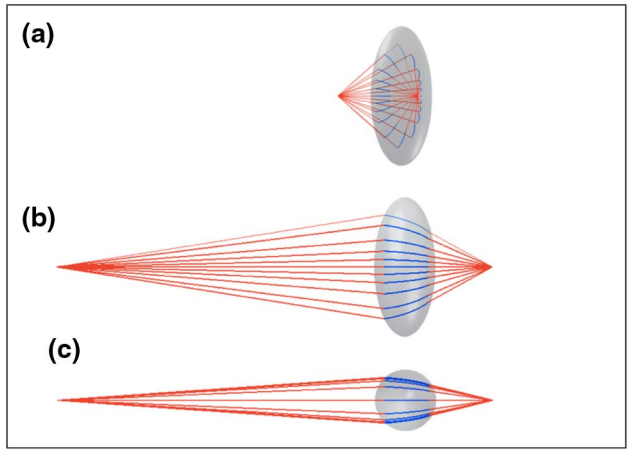

Fig. 10. 3D ray tracing in the generalized elliptical Luneburg lens with $P_0 = 5$. The 3D ray propagating is observed on (a) an angle that allows us to observe the 3D ray tracing, (b) the sagittal plane (zy plane), and (c) the tangential plane (zx plane).

wavefront for the first example and a spherical wavefront for the second example. A general example, where point P_0 is placed outside of the optical axis, is when a set of incident rays are associated with an helical wavefront, i.e., the rays are associated with a vortex beam. In this case, the rays are not coming from only point P_0, the rays are coming from different points of P_0 placed at different points of the 3D space, and the entry rays on the ellipse are skew rays, as shown in Fig. 11.

For the propagation in this example, it is necessary to use Eqs. (15) and (17) because the entry rays are not meridional rays. Note that the angle γ_r will take a different value for each incident ray, due to the value of γ_r, which is the same value of the inclination angle of each incident ray with respect to the zx plane; for this reason, each ray has a different propagation plane. If γ_r is known, then it is possible to know entry point P_{iL} on the surface of the elliptical Luneburg lens and the angle ϕ_r. Thus, it could be calculated with the equations, and it is possible to make the ray tracing of the incident skew rays inside the elliptical Luneburg lens, as is shown in the Fig. 12.

Figure 12 shows the propagation of three rays associated with a vortex beam. From this figure, it is possible to observe that the rays are not focusing in a single point, but this does not imply that the propagation is incorrect; this means that the propagation is correct because the rays associated with the vortex beam are coming from different points P_0.

Using the 3D ray tracing proposed in this paper, it is possible to analyze the ray propagation of any rays associated with a wavefront. The wavefront could be symmetric or asymmetric with respect to any of the three axis; for example, an aberrated wavefront could be analyzed. It is important to say that this analysis could not be made using 2D methods.

4. 3D RAY TRACING IN A COMPOSITE MODIFIED LUNEBURG MODEL OF HUMAN EYE LENS

The imaging capabilities of the CML lens and the changes in the gradient index profile were tested for five object distances, for a fixed geometry, and for a fixed image distance in [11]. The geometry proposed is defined by three shape parameters: the radius of the lens measured on the frontal plane (R), the anterior vertex (z_a), and the posterior vertex (z_p) where $z_p > z_a$, as shown in Fig. 13(a). The value of these shape parameters used in this model was reported in the literature by Rosen *et al.* in [20], and the idea of representing the GRIN distribution of the human eye lens as a GRIN distribution of the Luneburg lens, to the best of our knowledge, is attributed to Zainullin *et al.* in [21].

In the first case studied by Gómez-Correa *et al.* in [11], the CML lens is immersed in a refractive index of 1.336, which represents the aqueous humor of the human eye. The corresponding lens parameters for the sagittal plane are $R = 4.4005$ mm, $z_a = 1.8215$ mm, and $z_p = 2.5890$ mm ($z_a/z_p = 0.7036$), and the refractive index varies from 1.3998 in the center to 1.3709 in the surface of the CML lens. The entry parameters are $\alpha_0 = 0$ and $P_1 = 63.05$ mm.

To make the 3D ray tracing in the CML lens, it is necessary to define the tangential plane. Figure 13(b) shows that this

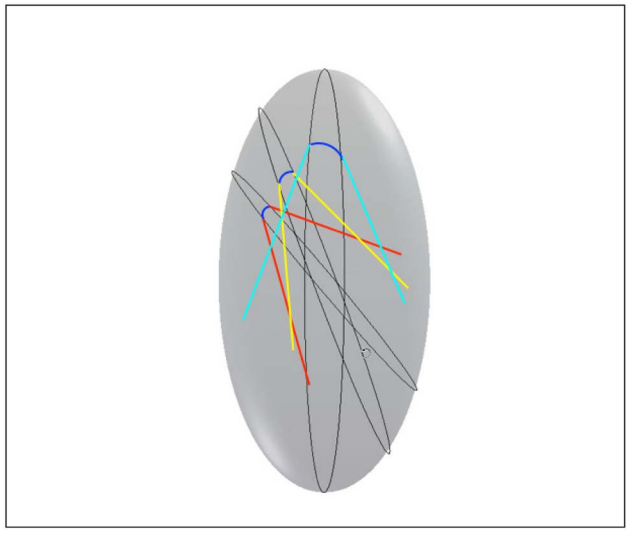

Fig. 12. Ray tracing of the associated rays to a vortex beam.

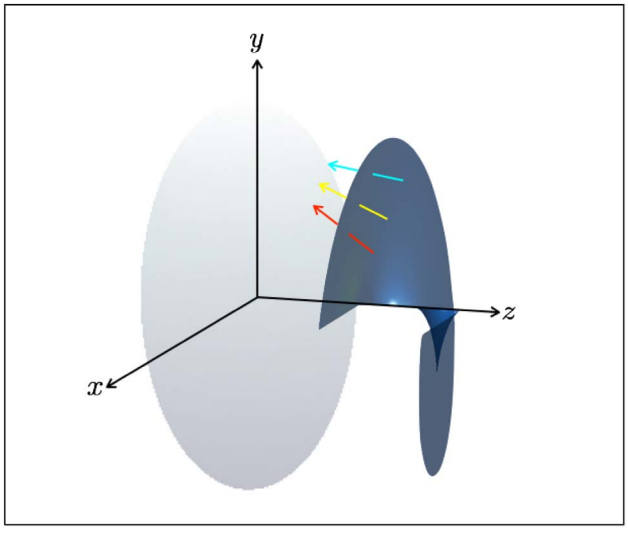

Fig. 11. Associated rays to a vortex beam.

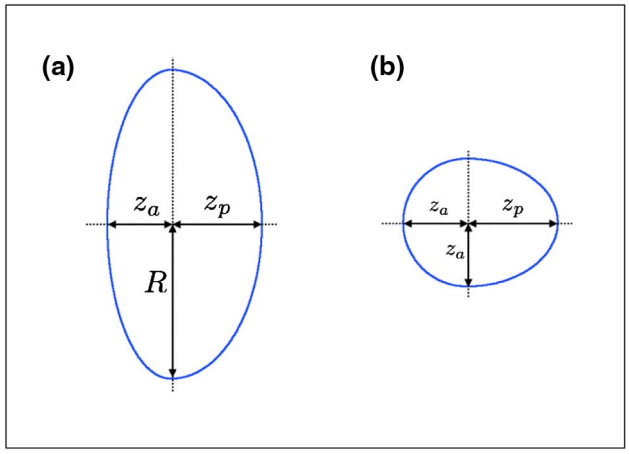

Fig. 13. Geometric shape of the CML lens. Parameters z_a and z_p are different.

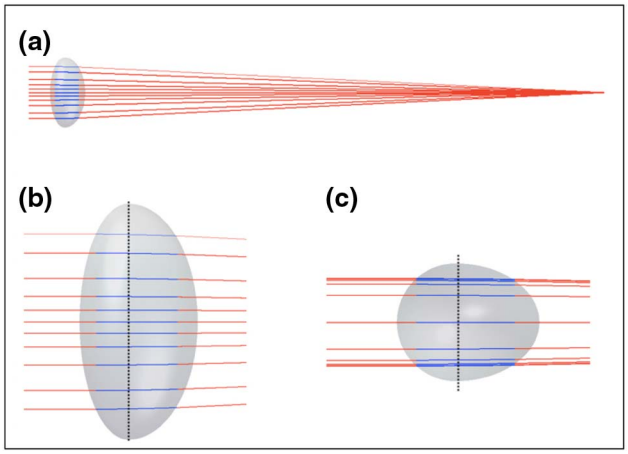

Fig. 14. Geometric shape of the CML lens. Parameters z_a and z_p are different.

plane is composed by the anterior and posterior hemispheres. The first is a semicircle with a radius of z_a, and the second is an ellipse with semiminor axis of z_a and semimajor axis of z_p. The value of z_a in the semiminor axis was chosen to show that the geometry of the CML lens in the tangential plane could be a circle in the anterior hemisphere and a ellipse in the posterior hemisphere. However, the value could be selected in different way: for example, by experimental data.

Using these parameters, the 3D ray tracing in the CML lens was performed, which is represented in Fig. 14(a). Ray tracing in the sagittal and the tangential planes are shown in Figs. 14(b) and 14(c), respectively. The rays have been cut because the focusing distances of the rays are large compared with the size of the CML lens.

In this propagation, it is possible to observe a difference between the value of the refractive index immerse and the value of the refractive index on the surface of the CML lens. However, the propagating rays inside the CML lens are not skew rays for two reasons: the first is due to point P_0 placed on the optical axis; the second is because the difference between the values of the refractive indexes are very small, i.e., this difference is 0.0349. This value is important when point P_0 is placed outside the optical axis. The analysis for this case is complicated by the generation of skew rays, and the geometry of the CML lens. Only one case of the five cases studied in [11] was presented, but it is possible to make 3D ray tracing of each case using the method presented in this paper.

5. CONCLUSIONS

A new method and the physical explanation of 3D ray tracing of generalized spherical and classical Luneburg lenses using 2D methods were presented.

It was observed that ray tracing is the same in each propagation plane in lenses with radial symmetry. This method takes advantage when the lens does not have a radial symmetry and also when the source point is placed outside of the optical axis because the ray tracing is different in each propagation plane. The physics of the problem have been analyzed in order to explain why, in the analysis presented in this paper, the skew rays are not generated inside the elliptical Luneburg lens and the basis for when the properties of the propagating rays as planar curves are preserved.

The method proposed could be used for circular and elliptical geometry or a composite of both with any gradient refractive index $n(r) = \sqrt{n_c - r^2}$, where $\sqrt{n_c}$ is the refractive index in the center of the lens. It is important to observe that the procedure of the method presented here is first to define the optics of the lenses and then to work out analytical ray tracing; however, it is possible to make the inverse analysis, i.e., if the ray tracing is known, then it is possible to find the optical characteristics of the lens that allow us to make the proposed ray tracing. An example of this is presented in [11] because the imaging capabilities of the CML lens and the changes in the gradient index profile are tested for five object distances, for a fixed geometry, and for a fixed image distance, i.e., the geometry of the lens and the object distance were known, and a GRIN distribution could be found that allows the ray tracing known for the object distance. Also, with this method, it is possible to fix the object distance to find a GRIN distribution and to establish the geometry of the lens.

Funding. Centro de Investigación Científica y de Educación Superior de Ensenada (CICESE)

Acknowledgment. The authors would like to acknowledge Nano-Optics Group of CICESE, Monterrey. The valuable comments by the referees helped to significantly improve the work here presented. The first author would like to acknowledge M. A. Canchola-Chávez and J. C. Melgarejo for fruitful discussions.

REFERENCES

1. R. K. Luneburg, *Mathematical Theory of Optics* (University of California, 1964).
2. R. Kingslake and R. Barry Johnson, *Lens Design Fundamentals* (SPIE, 2010).
3. A. Demetriadou and Y. Hao, "Slim Luneburg lens for antenna applications," Opt. Express **19**, 19925–19934 (2011).
4. J. A. Grzesik, "Focusing properties of a three-parameter class of oblate, Luneburg-like inhomogeneous lenses," J. Electromagn. Waves Appl. **19**, 1005–1019 (2005).
5. S. Ji, K. Yin, M. Mackey, A. Brister, M. Ponting, and E. Baer, "Polymeric nanolayered gradient refractive index lenses: technology review and introduction of spherical gradient refractive index ball lenses," Opt. Eng. **52**, 112105 (2013).
6. S. Ji, M. Ponting, R. S. Lepkowicz, A. Rosenberg, R. Flynn, G. Beadie, and E. Baer, "A bio-inspired polymeric gradient refractive index (GRIN) human eye lens," Opt. Express **20**, 26746–26754 (2012).
7. M. C. W. Campbell and A. Hughes, "An analytic, gradient index schematic lens and eye for the rat which predicts aberrations for finite pupils," Vis. Res. **21**, 1129–1148 (1981).
8. A. V. Goncharov and C. Dainty, "Wide-field schematic eye models with gradient-index lens," J. Opt. Soc. Am A **24**, 2157–2174 (2007).
9. R. Navarro, F. Palos, and L. González, "Adaptive model of the gradient index of the human lens. I. formulation and model of aging ex vivo lenses," J. Opt. Soc. Am A **24**, 2175–2185 (2007).
10. C. E. Jones, R. Meder, D. A. Atchison, and J. M. Pope, "Refractive index distribution and optical properties of the isolated human lens measured using magnetic resonance imaging (mri)," Vis. Res. **45**, 2352–2366 (2005).

11. J. E. Gómez-Correa, S. E. Balderas-Mata, B. K. Pierscionek, and S. Chávez-Cerda, "Composite modified Luneburg model of human eye lens," Opt. Lett. **40**, 3990–3993 (2015).
12. M. Bahrami and A. V. Goncharov, "Geometry-invariant GRIN lens: finite ray tracing," Opt. Express **22**, 27797–27810 (2014).
13. J. R. Flores, J. Sochacki, M. Sochacka, and R. Staroński, "Quasi-analytical ray tracing through the generalized Luneburg lens," Appl. Opt. **31**, 5167–5170 (1992).
14. J. R. Flores, "Gradient-index axicons with spherical symmetry," J. Mod. Opt. **46**, 1513–1525 (1999).
15. J. M. Gordon, "Spherical gradient-index lenses as perfect imaging and maximum power transfer devices," Appl. Opt. **39**, 3825–3832 (2000).
16. J. R. Flores, "Study of optical elements of gradient index with spherical symmetry," Ph.D. thesis (Universidade de Santiago, 1992).
17. S. P. Morgan, "General solution of the Luneburg lens problem," J. Appl. Phys. **29**, 1358–1368 (1958).
18. V. Lakshminarayanan, A. Ghatak, and K. Thyagarajan, *Lagrangian Optics* (Springer, 2001).
19. M. Born and E. Wolf, *Principles of Optics: Electromagnetic Theory of Propagation, Interference and Diffraction of Light*, 7th ed. (Cambridge University, 1978).
20. A. M. Rosen, D. B. Denham, V. Fernandez, D. Borja, A. Ho, F. Manns, J.-M. Parel, and R. C. Augusteyn, "In vitro dimensions and curvatures of human lenses," Vis. Res. **46**, 1002–1009 (2006).
21. R. G. Zainullin, A. B. Kravtsov, and E. P. Shaitor, "The crystalline lens as a Luneburg lens," Biofizika **19**, 913–915 (1974).